Nanoscale

Accepted Manuscript

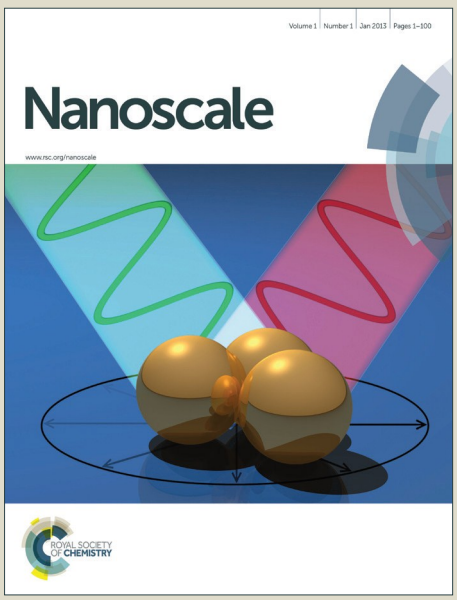

ROYAL SOCIETY OF CHEMISTRY

www.rsc.org/nanoscale

Nanoscale

RSCPublishing

ARTICLE

Facile Synthesis of Smart Magnetically Driven Fibrous Films for Remote Controllable Oil Removal†

Cite this: DOI: 10.1039/x0xx00000x

Jing Wu,[a] Nü Wang,[b] Yong Zhao*[b] and Lei Jiang[b,c]

Received 00th January 2012,
Accepted 00th January 2012

DOI: 10.1039/x0xx00000x

www.rsc.org/

Inspired by the marine mussel adhesive protein, the smart magnetic controllable oil adsorption nanofibrous materials were successfully fabricated in this work. Taking advantages of dopamine which molecular structure mimics the single unit of marine mussel adhesive protein and can be polymerized in alkaline solution forming a "glue" layer on many kinds of material surfaces, magnetic Fe_3O_4 nanoparticles were easily and robustly anchored on the electrospun polyvinylidene fluoride (PVDF) fibrous films. After fluorination, the as-prepared hierarchical structured films exhibited superhydrophobicity, superoleophilicity and excellent oil adsorption capacity from water. Importantly, due to the magnetic controllable property endowed by Fe_3O_4 nanoparticles, such fibrous films act as the "smart magnetic controlled oil removal carrier", which effectively overcome the drawback of the only *in situ* oil adsorbed materials and can be retrieved easily. Such facile strategy will extend the fabrications of intelligent oil-water separation materials as well as cater and board the practical applications in the remote controlled oil-water separation areas.

Introduction

With the acceleration of industrialization process, oil exploration, transportation, storage, usage as well as oily sewage emissions have engendered many oil spills which not only bring about serious damages to natural environment, but also cause a great loss of energy.[1-3] Fully cognized of their hazards, three main classes of oil adsorbent materials: inorganic mineral products, organic natural products, and synthetic organic products combined with numerous fabrication routes, such as template-based techniques,[4] self-assembly of block co-polymers,[5] layer-by-layer assembly,[6] supercritical drying,[7] electrochemical etching,[8] et al., were applied to govern the oil spills. Recently, taking advantages of design and fabrication special wettability materials (superhydrophobicity/superoleophilicity or superhydrophilicity/superoleophobicity) by tailoring the chemical compositions and surface structures, a variety of oil-water separation materials that can selectively concentrate, adsorb or filtrate oil (or water) have been successfully obtained.[9-22] Due to the different wetting essences towards oil and water, they exhibit higher oil-water separation efficiency than other tradition materials. However, although in terms of higher separation efficiency, such materials show distinct disadvantages for they can only be used *in situ*. When in the case of an urgent need for the intelligent remote controllable operation, the applications of them are restrained.

In order to cater the increased intelligent requirements in practical applications, smart oil adsorbed material that can be responsive to the external stimulations and act as "oil controlled carrier" is an ideal one. It shows great advantages not only on accelerating separation rate, but also on controllable oil collection. Unfortunately, only few works, such as smart textiles that provide controllable and switchable adsorption to oil in different pH value aqueous solutions by grafting pH-responsive polymer[23], and adsorptive powers by mixing magnetic particles[24-28], were concentrated on these smart oil adsorbed materials[29]. In this work, the fabrication of smart magnetic responsive oil adsorbed fibrous film via facile electrospinning method has been firstly reported. Inspired by the marine mussel which can keep long-lasting adhesion in wet environment resulted from the adhesive proteins containing high levels of dopamine (3,4-dihydroxy-phenylalanine)[30], magnetic Fe_3O_4 nanoparticles were easily and robustly anchored on the electrospun nanoscaled polyvinylidene fluoride (PVDF) fibrous films in mild condition. After fluorination, the electrospun fibrous films not only exhibit superhydrophobicity, superoleophilicity and efficient oil adsorption ability, but also reveal smart magnetic responsive property, which can controllably and selectively adsorb oil from many kinds of oil-water mixtures. Combined with the facile and large-scaled processable fabrication methods, such superhydrophobic/superoleophilic magnetic responsive fibrous materials can be used as the oil adsorbed fibrofelt and exhibit great potential in the application of remote controllable oil removal field.

Experiment

Preparation of polyvinylidene fluoride (PVDF) fibers: PVDF ($M_w \approx 180{,}000$, Sigma-Aldrich) was dissolved in DMF (Beijing Yili Fine Chemical Co.) by stirring for 6 h to form 18 wt% precursor solution. Nearly 3 mL precursor solution was placed in 5 mL syringe. In order to form PVDF fibers with different diameters, different metal needles of 0.6 mm, 0.8 mm, 1.0 mm, and 1.2 mm inner diameter were equipped. A stainless steel plate covered with a sheet of non-woven fabrics was employed as the collector. The distance between the needle tip and collector was 20 cm, and the voltage was set as 15~20 kV. The samples were named PVDF-6, PVDF-8, PVDF-10 and PVDF-12, respectively.

Anchoring Fe_3O_4 nanoparticles on electrospun PVDF fibrous film and fluorination: The as-prepared PVDF fibrous films were cut into squares (3 cm × 3 cm) and ultrasonically cleaned by water and ethanol. Meanwhile the Fe_3O_4 nanoparticles (Aladdin Co.,) were washed by ethanol several times. 80 mg Fe_3O_4 nanparticles and 80 mg dopamine hydrochloride were dispersed in 40 mL Tri-HCl solution (10 mM, pH = 8.5). The cut piece of PVDF film was immersed in the above solution stirring for 24 h. Then the as-prepared samples were washed by ethanol to wipe off the residual Fe_3O_4 nanoparticles. Finally, the as prepared samples were dipped into the 1H,1H,2H,2H-perfluorodecanethiol (Sigma-Aldrich) ethanol solution (1:500) for 12 h and dried at 60℃.

Instruments and Characterization: SEM images were taken by scanning electron microscope. (JSM-6700F, Japan). The diameter of the fibers was measured on the basis of SEM images. Contact angles were measured on an OCA 20 contact-angle system (Dataphysics, Germany) at 25□. 2 μL deionized water and n-hexane droplets were dropped onto the surface, respectively. The average contact angle value of both water and oil were obtained by measuring at five different positions of the same sample. The water adhesion forces were measured using the high-sensitivity micro-electro-mechanical balance system (Data-Physics DCAT11, Germany), 1, 2-dichloroethane was chosen as the detected oil. A 5 μL 1, 2-dichloroethane droplet was suspended with a metal cap and controlled to contact with the surface of the film with a constant speed of 0.02 $mm \cdot s^{-1}$ and then controlled to leave. X-ray diffraction (XRD) were collected on a Rigaku-D/max 40,000 V X-ray diffractometer equipped with Cu Kα radiation (λ = 0.15418 nm) at a step width of 5°/min. The Vibrating sample magnetometer (VSM, Lake shore 7400) was utilized to examine the magnetic properties of as-prepared samples. Fourier transform infrared (FT-IR) spectra were obtained with a Bruker-EQuiNOX55 spectrometer. X-ray photoelectron spectroscopy (XPS) data were obtained by an ESCALab220i-XL electron spectrometer from VG Scientific using 300 W AlKα radiation, and the base pressure was about 3×10^{-9} mbar.

Oil absorption tests: In order to analyze the maximum oil sorption capacity of PVDF sorbents, 1.0 g of oil sorbent was placed in a glass beaker filled with 100 mL of oil. After 40 min of sorption, the wet sorbent was drained for 5 min until no residual oil droplet left on the surface. Oil sorption capacity of all sorbents was determined by the following equation:

$$q = \frac{[m_f - (m_0 + m_w)]}{m_0}$$

Where q is the sorption capacity (g/g), m_f is the weight of the wet sorbent after 5 min of drainage (g), m_0 if the initial weight of the sorbent (g), and m_w is the weight of absorbed water (g). In the pure oil medium without any water, m_w is equal to zero. To determine the selectivity absorptive capacity of the fibrous film sorbents, 0.1 g as-prepared sorbents were placed in oil/water mixture. The weight rations between oil and water was 1: 10. After 20 min of absorption, wet sorbents were removed, drained for 5 min, and weighed.

Results and Discussion

Synthesis of magnetic anchored PVDF fibrous film

Due to the excellent chemical, oxidative, high shock and solvent resistance properties, polyvinylidene fluoride (PVDF) is a common used material for filtration, distillation, structural material coating applications, etc.[31-34] In this work, the fibrous PVDF films were facilely fabricated via electrospinning. Inspired by the strong and long-lasting bioadhesion of marine mussels in wet environment, dopamine, which molecular structure mimics the single units of mussel adhesive protein, was used to directly anchor magnetic Fe_3O_4 nanoparticles on the electrospun PVDF fibers' surfaces. Due to the strong covalent and noncovalent interactions with surfaces, dopamine can form "glue" layers virtually in all kinds of material surfaces in alkaline solution during the process of polymerization. The typical fabrication process is shown in Scheme 1. After electrospinning, the PVDF fibrous films were immersed in the stirred Tris(hydroxymethyl) aminomethane hydrochloride (Tris-HCl) aqueous solution (pH=8.5), of which contained dopamine (DOPA) and Fe_3O_4 nanoparticles. In such weak alkaline solution, DOPA was polymerized during the oxidation process to form polydopamine (PDA) layers on both fibrous film and Fe_3O_4 nanoparticles surfaces. Hence, magnetic Fe_3O_4 nanoparticles were robustly glued on the PVDF fibrous film even then washed by diluted water and ethanol several times. After 1H, 1H, 2H, 2H-perfluorodecanethiol (PFDT) fluorination, superhydrophobic/superoleophilic Fe_3O_4 anchored PVDF fibrous film (Fe_3O_4@PVDF/F) was successfully obtained.

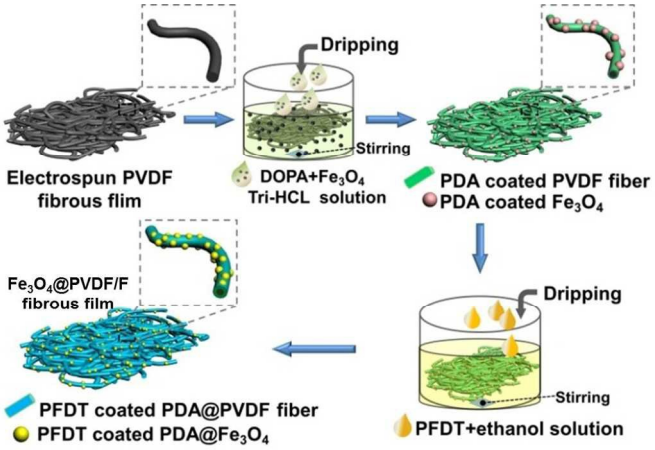

Scheme 1. Schematic illustration of the superhydrophobic and superoleophilic Fe_3O_4@PVDF/F fibrous film fabrication process. The electrospun PVDF fibrous films were immersed in the stirred Tris-HCl aqueous solution containing DOPA and Fe_3O_4 nanoparticles. DOPA was polymerized to form PDA layers on both fibrous film and Fe_3O_4 nanoparticles surfaces, which can robustly glue magnetic Fe_3O_4 nanoparticles on the PVDF fibrous film. After fluorination, the Fe_3O_4@PVDF/F fibrous film was formed.

According to Fig. 1(a), when magnetic field applied, the as-prepared film tightly adsorbed on the magnet, which shows magnetic responsive essence. Fig. 1(b) exhibits the wetting behaviour of both water and oil on such prepared film. The film surface shows a water contact angle about 155° and an oil contact angle near to 0°, respectively, indicating superhydrophobicity and superoleophilicity. Furthermore, through morphology observation, it can be seen clearly that the PVDF fibers are randomly oriented on the scaffold forming a compact nanofibrous film, and the magnetic Fe_3O_4 nanoparticles with octahedral shape are anchored on fibers' surfaces (Fig.1(c)).

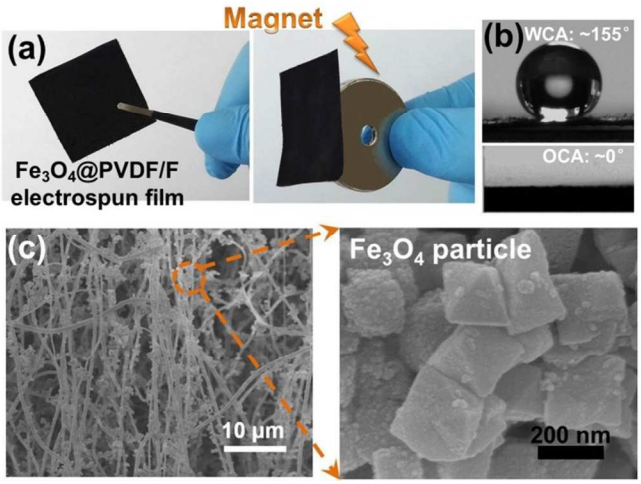

Fig.1 (a) Photographs of Fe_3O_4@PVDF/F fibrous film. To obtain a clear view, a square piece of the sample consisted of several layers of Fe_3O_4@PVDF/F-6 films folded and pressed together was used. The sample shows dark black (Left). When in the magnetic field, such film tightly adsorbs on the magnet (Right). (b) Water and oil contact angles of the sample. The fibrous film exhibits superhydrophobicity and superoleophilicity. (c) SEM images of as-prepared fibrous film and the anchored magnetic Fe_3O_4 nanoparticles.

Morphology and structure of Fe_3O_4@PVDF/F fibrous film

As showing in Fig. 2, scanning electron microscopy (SEM) was used to characterize the morphologies and structures of all prepared samples. To investigate the influence of different fibers' morphologies to the oil adsorption capacity, metal needles with different inner diameters, 0.6 mm, 0.8 mm 1.0 mm and 1.2 mm, were equipped during the electrospinning process. Accordingly, Fig.2 (a), (c), (e), (g) are the typical SEM images of pure electrospun PVDF fibrous film (named PVDF-6, -8, -10 and -12). Meanwhile, the Fe_3O_4 anchored samples corresponded to the different diameters mentioned above are showing in Fig.2(b), (d), (f), (h) (named Fe_3O_4@PVDF/F-6, -8, -10 and -12). For both the pure PVDF and Fe_3O_4 anchored samples, the fibers are randomly oriented on the scaffold. Compared with the electrsopun PVDF-6, PVDF-8, PVDF-10, PVDF-12, of which the statistic average diameters are 190 nm, 205 nm, 242 nm and 318 nm, respectively, the average diameters of Fe_3O_4 anchored samples are increased to 214 nm, 234 nm, 362 nm and 397 nm, respectively. It can be attribute to the spontaneous polymerization of dopamine which resulted in a thin polymer layer deposited on the eletrsopun PVDF fibers.[30]

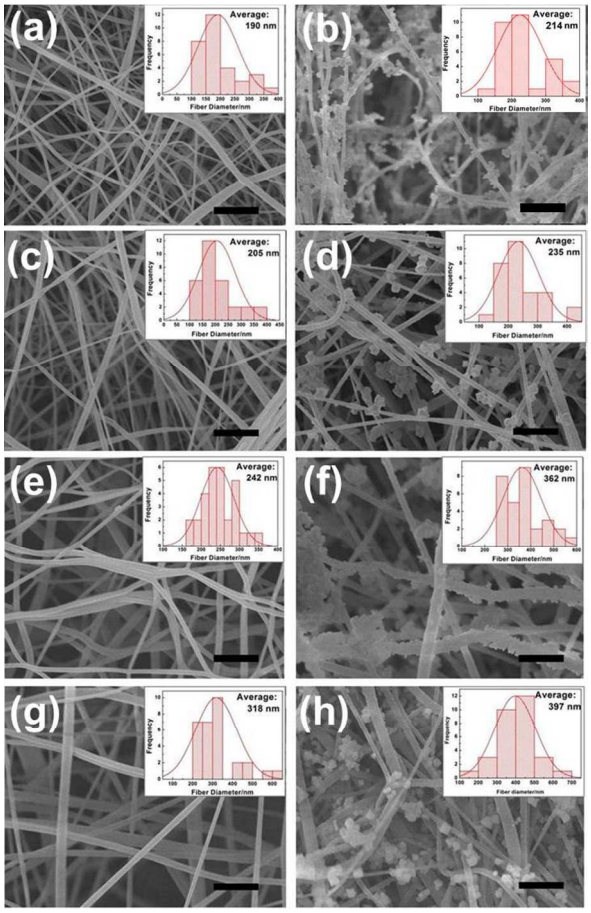

Fig.2 SEM images and fiber diameter distribution statistics of the as-prepared samples. (a),(c),(e),(g) The pure PVDF-6, -8, -10 and -12 electropun fibers. The average fiber diameters are 190 nm, 205 nm, 242 nm and 318 nm, respectively. (b), (d), (f), (h) Fe_3O_4@PVDF/F-6,-8,-10 and -12 electrospun fibers. The average fiber diameters are 214 nm, 234 nm, 362 nm and 397 nm, respectively.(Bar: 2 μm)

Wettability of as-prepared samples

The influence of fibers' diameter to the film wettability was investigated. When a water droplet about 2 μL allowed to contact the surfaces, the water contact angles are 154.9° ± 0.6°, 152.6° ± 1.3°, 151.1° ± 0.4° and 150.2° ± 0.7° for Fe_3O_4@PVDF/F-6, Fe_3O_4@PVDF/F-8, Fe_3O_4@PVDF/F-10, Fe_3O_4@PVDF/F-12, respectively, indicating that all magnetic Fe_3O_4 nanoparticles anchored fibrous sorbent films are superhydrophobicity, and the water contact angle decreased slightly with the increased average fiber diameters (Fig. 3(a)). It can be attributed to that for a fibers-composed surface, the smaller fiber diameter usually brings about greater surface roughness, which can enhance the wetting behaviour of a liquid on a solid. When oil droplet (1,2-dichloroethane, 2 μL) dropped on each sample surfaces mentioned above, all droplets immediately spread on the film with a contact angle near to 0°, which show that all samples are superoleophilicity (more details can be seen in ESI S1†). Meanwhile, taking Fe_3O_4@PVDF/F-6 as an example, the adhesion force between water and film surface was measured dynamically. A water droplet (5 μL) was contact to fibrous film surface and then made it leave. The adhesive force was recorded by a high-

sensitivity microelectromechanical balance system. The water adhesive force of the electrospun pure PVDF fibrous film was 10.3 ± 1.8 μN (Fig. 3b, Top). After Fe_3O_4 anchoring and fluorination, there is no detectable data, indicating an extremely low adhesive force (Fig. 3b, Bottom). When oil droplet contacted to the sample surface, it spread on the surface and be adsorbed by the film rapidly. These characteristics are advantages for the magnetic fibrous film to anti-water and adsorb oil effectively. The Fe_3O_4 anchored samples also exhibit good mechanical strength with the average tensile strength of 22.54±1.12 MPa and elongation at break of (57.47±3.33)% (see details ESI S2†).

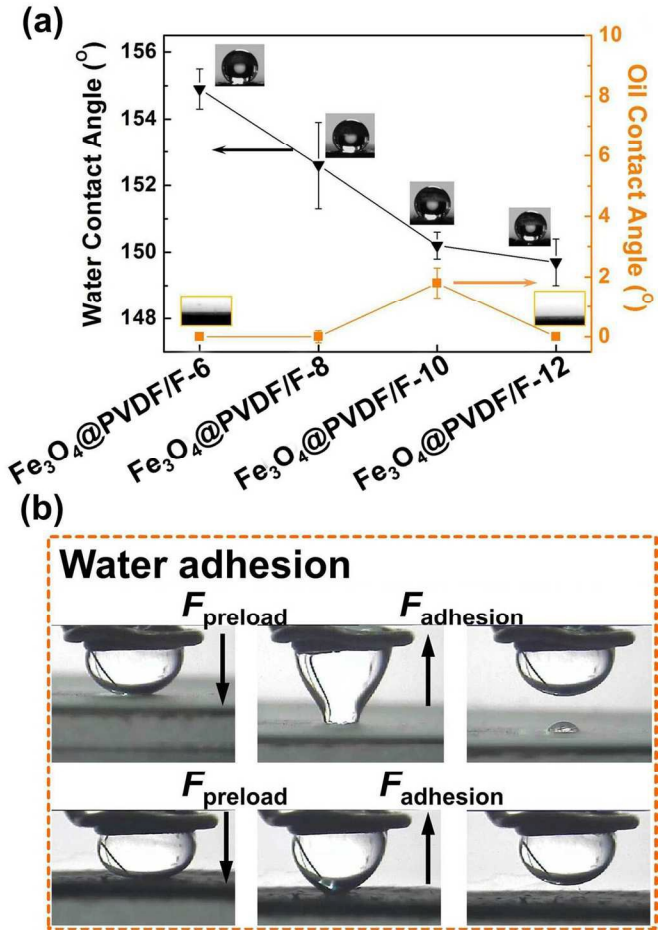

Fig. 3 (a) Variation of water contact angles and oil contact angles of Fe_3O_4@PVDF/F electrospun fibrous films with different fiber diameters. (Oil: 1,2-dichloroethane, 2 μL). (b) Photographs of water droplets, taken at different stages during the adhesive force measurement process on electrospun PVDF fibrous film (Top) and Fe_3O_4@PVDF/F-6 fibrous film (Bottom).

Crystal structures and magnetic properties

During the fabrication process, XRD patterns were used to exam and confirm the crystal forms as well as the polymorphism of pure PVDF fibrous film, magnetic Fe_3O_4 nanoparticles, dopamine and Fe_3O_4@PVDF/F (Fig. 4(a)). It is well known that PVDF adopts one of the following three crystalline structures: Form I (β-type crystal with planar zigzag conformation, orthorhombic), Form II (α-type crystal with TGTĞ, monoclinic) and Form III (γ-type crystal with TTTGTTTĞ, monoclinic).[35-37] In our case, the as-prepared PVDF electrospun fibrous film exhibits broader peaks, and two obvious characteristic peaks are located at 18.4° and 21.0°, which may indicate that the crystal structure of PVDF fibrous film is amorphous or partially collapses. Meanwhile, according to the result, the magnetic Fe_3O_4 nanoparticles shows face-centered cubic phase of magnetite characterized by the 2θ values of 30.12°(220), 35.44°(311), 37.12°(222), 43.12°(400), 53.4°(422), 57.0°(511) and 62.56°(440).[38,39] The peak positions of Fe_3O_4@PVDF/F located at 35.44°, 43.12°, 53.4°, 57.0° and 62.56° match well with those of magnetic Fe_3O_4 nanoparticles.

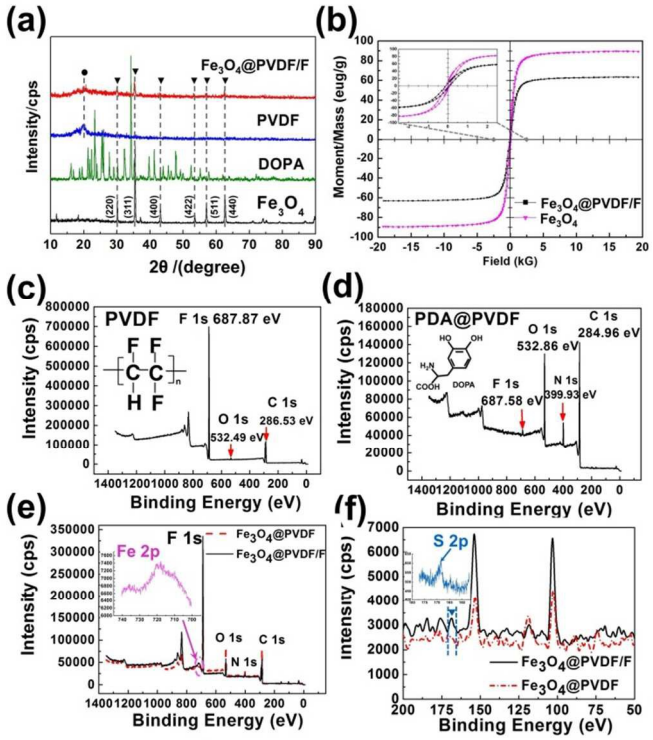

Fig. 4 (a) XRD patterns of Fe_3O_4 nanoparticles, DOPA, PVDF and Fe_3O_4@PVDF/F samples. (b) The hysteresis loops of Fe_3O_4 nanoparticles and Fe_3O_4@PVDF/F-6 samples (Insertion: Magnification part in the range of -2.5 kG to 2.5 kG). (c, d) Full XPS spectrum of both pure PVDF electrospun fibrous film and PDA@PVDF. The intensity of F 1s characteristic peak decreases sharply, and the new peak contributing to N 1s appears. (e) Full spectrums of Fe_3O_4@PVDF and Fe_3O_4@PVDF/F films. Fe 2p peaks appear on both samples. (f) Partial magnification of (e), ranging from 200 eV to 50 eV. The new weak peak located at 168.39 eV (Insertion) in Fe_3O_4@PVDF/F spectrum is corresponded to S 2p.

Along with the dopamine and PVDF for comparison, the spectrum of Fe_3O_4@PVDF/F keeps the same with that of pure PVDF, and no dopamine characteristic peak appears, but only adds magnetic Fe_3O_4 nanoparticles characteristic peaks. It demonstrates that dopamine does not affect the crystallization structures of Fe_3O_4@PVDF/F fibrous film, just only act as the "glue" that stick magnetic Fe_3O_4 nanoparticles on electrospun fibers' surfaces. In order to test the magnetic property of Fe_3O_4 and Fe_3O_4@PVDF/F, vibrating sample magnetometer (VSM)

was used. As shown in Fig.4(b), the magnetization, coercivity and residual magnetization for both Fe_3O_4 and Fe_3O_4@PVDF/F samples are 89.625 emu/g, 9.9138 emu/g, 90.522 G and 63.343 emu/g, 5.714 emu/g, 88.094 G, respectively, which make a clear view that both the Fe_3O_4 nanoparticles and Fe_3O_4@PVDF/F fibrous film exhibit hysteresis phenomenon (Fig. 4(b), Insertion). Such above results indicate that although the magnetism of Fe_3O_4@PVDF/F fibrous film is lower that of pure Fe_3O_4 nanoparticles, it is also superparamagnetism which endows magnetic essence to such as-formed films.

Chemical composition characterization

XPS was used to probe chemical compositions of the outermost 5-10 nm of the as-prepared samples in the fabrication process. For the PVDF, dopamine decorated film (PDA@PVDF), Fe_3O_4@PVDF and Fe_3O_4@PVDF/F samples, unambiguous differences can be observed. The C 1s, O 1s and F 1s characteristic peaks of electrospun PVDF fibrous film are shown in Fig. 4(c) as a basic standard for comparison. During the dopamine decoration and polymerization process,[40-45] since dopamine changed to polydopamine in weak alkali solution environment, a thin layer of polydopamine was coated on fiber surface, caused the new peak attributed to N 1s (399.93 eV) appeared, and the intensity of F 1s decreased as well as O 1s increased (Fig. 4(d)). When Fe_3O_4 nanoparticles were "glued" on the PDA@PVDF fibrous film, a wide peak located at 720.72 eV can be observed for both Fe_3O_4@PVDF and Fe_3O_4@PVDF/F samples (Fig. 4(e) and Insertion). This signal peak can be attributed to Fe^{3+} 2p3/2, which matches to the some reported literatures.[38, 46-48] The Fe^{3+} tetrahedral species has a binding energy of 719.55 eV. The binding energy of Fe 2p 3/2 is 707.95 eV and binding energy of Fe 2p 1/2 is 719.55 eV, which corresponded to the XPS spectrum of Fe_3O_4 with satellite peak at 718.80 eV (ESI S3†). According to Fig. 4(e) insertion, Fe characteristic peaks consistent of many noise peaks, which can be contribute to the strong magnet interference to the field emission XPS equipment. Meanwhile, compared with the unmodified sample, the signal of F 1s for Fe_3O_4@PVDF/F is significant enhanced. In addition, as showing in Fig. 4(f), after surperhydrophobic modification by 1H, 1H, 2H, 2H-perfluorodecanethiol, the weak peak located at 168.39 eV appeared in the spectrum of Fe_3O_4@PVDF/F. It is the S 2p signal, which demonstrates the successful fluorination modification.[49]

Oil removal capacity

Efficient oil adsorption combined with magnetic responsive capacity is expected to be the great potential for the application of remote controlled oil-water separation. In our study, the magnetic controllable oil adsorption capacities of as-prepared superhydrophobic/superolephilic Fe_3O_4@PVDF/F electrospun fibrous films were tested. As shown in Fig. 5(a), a square piece of the magnetic fibrous film consisted of several layers of Fe_3O_4@PVDF/F-6 films folded and pressed together was used as an example. By simply placing to the oil/water mixture, the film floats on the surface, touches the oil and adsorbs it from the mixed solution quickly. When magnetic field applied, the film exhibits magnetic responsive capacity that fibrous film which adsorbed certain amount of oils moved toward to the magnetic field. Such fibrous film can be controlled by magnet, inaugurating a novel way for controllable oil removal.

In Fig. 5(b) and (c), the oil adsorption capacities of both non-decorated PVDF fibrous films and the Fe_3O_4@PVDF/F films were measured. Six kinds of oils which are typically used in industry and daily life were applied as the oil solvents. According to Fig. 5(b), among all samples with different fiber diameters, the PVDF-6 exhibits the highest oil adsorption capacity which may attribute to the increased specific surface areas caused by the decreased fiber diameter.[50] The oil adsorption capacities change as the following orders: motor oil ＞soybean oil＞silicon oil＞diesel oil＞n-hexane＞gasoline. The different oil adsorption capacities can be attributed to the viscosity and surface tension of such oils. Taking into consideration of high viscosity, it leads to two effects, which are the relation of a mutual competition. One is the enhanced effect. That is it can increase the adsorption capacity by improving the adherence of oil onto the fiber surface. The other is inhibition effect that the adsorption capacity can be decreased for heavier oil inhibiting the oil penetration into the interior of film sorbents. The oil properties are listed in ESI S4†. The oil adsorption capacity mentioned above is agreed with the decreasing tendency of oil viscosity. Meanwhile, surface tension is the resultant intermolecular force when one fluid exerts on anther surface or liquid. Low value of surface tension suggests that oil could penetrate the sorbents and remain trapped with the solid sorbent. Herein, the oils we chosen show inconspicuous difference between their surface tension but obvious different in viscosity. Accordingly, in our study, the low surface energy of as-mentioned oil solvents give rise to superoleophilicity and adsorption capacity, and the oil solvent viscosity plays an dominant role in the difference of adsorption capacities.

Compared to the non-decorated PVDF fibrous film, the oil adsorption capacities of all Fe_3O_4@PVDF/F samples are nearly 1.5-2 times higher and show adsorption capacity up to about 8-30 times over their own weights (Fig.5(c)). After Fe_3O_4 nanoparticles anchoring and 1H, 1H, 2H, 2H-perfluorodecanethiol fluorination, the wetting and anti-wetting abilities of the as-prepared films enlarged due to both the hierarchical structures formation by which increased the surface roughness, and chemical composition change that lower the surface energy.[51-53] According to the R. N. Wenzel theory, the roughness factor is the ration between the actual surface area and the geometric surface area of a rough surface.[54] Therefore, for the fiber-nanoparticle composited surface, the smaller fiber diameter and smaller nanoparticle size can bring about greater roughness. It not only endows enlarged superhydrophobicity /superoleophilicity, but also increases the specific surface areas. Such enlarged superhydrophobicity/superoleophilicity and specific surface area can improve the oil adsorption capacity in oil/water mixed system. Taking Fe_3O_4@PVDF/F-6 for example, the oil adsorption capacities of motor oil, soybean oil, silicon oil, diesel oil, n-hexane and gasoline are 30.96 ± 1.15, 26.79 ± 0.84, 23.05 ± 0.42, 12.11 ± 0.63, 9.37 ± 0.73 and 7.0 ± 1.29 g/g, respectively, and the oil adsorption capacity change order is the same as the pure PVDF samples. That is, the Fe_3O_4 anchoring not only enhances the oil adsorption capacity by enlarging the film surface roughness and the specific surface area, but also endows magnetic responsive ability which expands its applications especially in remote controllable oil removing.

After oil adsorption, large amount of such adsorbed oils can be collected easily by simple extruding or centrifugal separation. Fig. 5(d) shows the stabilization and reutilization of Fe_3O_4@PVDF/F-6 during 5 cycles, there is no evidently

changes on adsorption capacity and fibrous structures (ESI S5†). Furthermore, compared with the water and oil contact angles as well as water sliding angles before and after 5 cycles usage, all of them are not evidently changed, which make the samples promising candidate for oil removal in reality (ESI S6† and S7†).

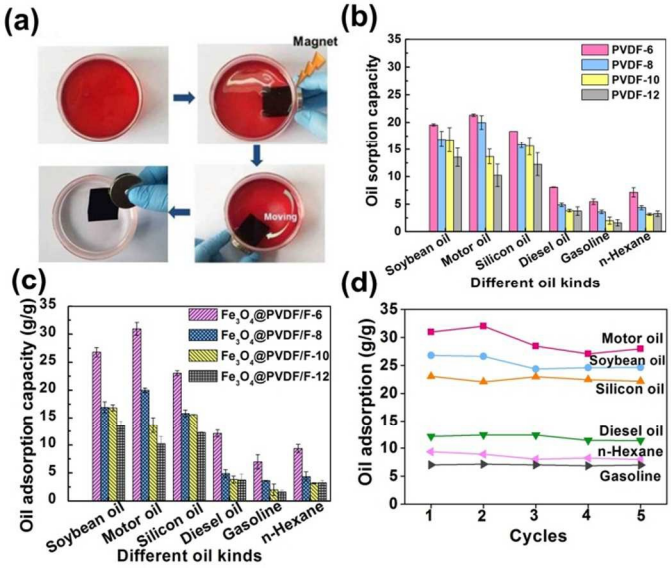

Fig. 5 (a) Snapshots of magnetic driven oil removal capacity of the Fe_3O_4@PVDF/F fibrous film. When the sample was deposited on the oil/water bath, it adsorbed the red colored motor oil (dyed with Oil Red O). Once magnetic field applied, the film moved toward to the magnetic field direction, driving oil along with it, and could be hang it up by magnet. (b) Oil adsorption capacities of the electrospun PVDF fibrous film with different fiber diameters. For all samples with different fiber diameters, the adsorption capacity for six kinds of oil decreased as the following order: motor oil＞soybean oil＞silicon oil＞ diesel oil ＞ gasoline ＞ n-hexane. (c) The oil adsorption of Fe_3O_4@PVDF/F samples with different fiber diameters. The Fe_3O_4@PVDF/F-6 exhibits the highest oil adsorption capacity. (d) Recycle utilization characterization of Fe_3O_4@PVDF/F-6 fibrous film. Weight gains for six kinds of different oils were recorded after adsorption and desorption for five cycles.

Conclusion

In summary, taking inspiration of the strong adhesion essence of marine mussel protein from nature, magnetic Fe_3O_4 nanoparticles are successfully anchored on the electrospun PVDF fibrous films in mild condition, forming hierarchical superhydrophobic/superoleophilic fibrous films. Due to the magnetic responsive capacity bestowed by Fe_3O_4 nanoparticles, the as-prepared fibrous films exhibit smart magnetic responsive capacity and can be act as the "oil controlled carriers", which are the ideal candidates in the application of remote controllable oil-removing areas. Such approach might be extended to various extreme environments, e.g., polluted water areas that do harm to workers' safety if they get close to. This work provides a new insight to the fabrication of low-cost, high efficient and smart responsive oil adsorption material through convenient way, overcome the hard design and fabrication of smart responsive oil/water separation materials.

Acknowledgements

The authors acknowledge the NSFC (21134003, 21222309, 21374001), 863 Program (2013AA031903), 973 Program (2012CB933200), Natural Science Foundation of Beijing (Grant No. 2154047), the Open Project Program of Beijing Key Laboratory (Grant No. 2013ZK-01), the Project of Young Scientific Research Innovation Found of Beijing Institute Fashion Technology (Grant No. AK2014-22), and Research Project of Talent Introduction Found of Beijing Institute Fashion Technology (Grant No. 2014A-21).

Notes and references

[a] College of Material Science and Engineering, Beijing Institute of Fashion Technology, Beijing 10029, P. R. China;
Beijing Key Laboratory of Clothing Materials R&D and Assessment, Beijing 100029, P. R. China.
[b] Key Laboratory of Bio-Inspired Smart Interfacial Science and Technology of Ministry of Education, School of Chemistry and Environment, Beihang University, Beijing 100191, P. R. China.
[c] Beijing National Laboratory for Molecular Sciences (BNLMS), Key Laboratory of Organic Solids, Institute of Chemistry, Chinese Academy of Sciences, Beijing 100190, P. R. China.

† Electronic Supplementary Information (ESI) available: The comparison of water contact angles (oil contact angles) between Fe_3O_4@PVDF/F and PVDF fibrous films, mechanical property, Fe 2p spectrum, oil physical properties, the structure comparison between and after oil adsorption, water contact angles (oil contact angles) before and after utilizations, and water sliding angles of Fe_3O_4@PVDF/F-6 before and after 5cycles usage are given in the Electronic Supplementary Information. See DOI: 10.1039/b000000x/

1. A. B. Nordvik, J. L. Simmons, K. R. Bitting, A. Lewis and T. S. Kristiansen, *Spill Sci. Technol. B*, 1996, 3, 107-122.
2. B. M. Jenssen, *Environ. Pollut.*, 1994, 86, 207-215.
3. S. S. Madaeni and M. K. Yeganeh, *J. Porous Mat.*, 2003, 10, 131-138.
4. Y. L. Zhang, S. Wei, F. J. Liu, Y. C. Du, S. Liu, Y. Y. Ji, T. Yokoi, T. Tatsumi and F. S. Xiao, *Nano Today*, 2009, 4, 135-142.
5. H. S. Mansur, R. L. Oréfice and A. A. P. Mansur, *Polymer*, 2004, 45, 7193-7202.
6. M. Cheng, Y. Gao, X. Guo, Z. Shi, J. f. Chen and F. Shi, *Langmuir*, 2011, 27, 7371-7375.
7. A. V. Rao, N. D. Hegde and H. Hirashima, *J. Colloid. Interf. Sci.*, 2007, 305, 124-132.
8. D. D. La, N. Tuan Anh, S. Lee, J. W. Kim and Y. S. Kim, *Appl. Surf. Sci*, 2011, 257, 5705-5710.
9. M. H. Jin, J. Wang, X. Yao, M. Y. Liao, Y. Zhao and L. Jiang, *Adv. Mater.*, 2011, 23, 2861-2864.
10. Z. Xue, S. Wang, L. Lin, L. Chen, M. Liu, L. Feng and L. Jiang, *Adv. Mater.*, 2011, 23, 4270-4273.
11. G. Kwon, A. K. Kota, Y. X. Li, A. Sohani, J. M. Mabry and A. Tuteja, *Adv. Mater.*, 2012, 24, 3666-3671.
12. Z. Xue, Z. Sun, Y. Cao, Y. Chen, L. Tao, K. Li, L. Feng, Q. Fu and Y. Wei, *RSC Advances*, 2013, 3, 23432-23437.
13. X. Zhang, Z. Li, K. Liu and L. Jiang, *Adv. Funct. Mater.*, 2013, 23, 2881-2886.

14. W. Zhang, Z. Shi, F. Zhang, X. Liu, J. Jin and L. Jiang, *Adv. Mater.*, 2013, 25, 2071-2076.
15. Z. Shi, W. Zhang, F. Zhang, X. Liu, D. Wang, J. Jin and L. Jiang, *Adv. Mater.*, 2013, 25, 2422-2427.
16. F. Zhang, W. B. Zhang, Z. Shi, D. Wang, J. Jin and L. Jiang, *Adv. Mater.*, 2013, 25, 4192-4198.
17. W. Zhang, Y. Zhu, X. Liu, D. Wang, J. Li, L. Jiang and J. Jin, *Angew. Chem. Int. Edit.*, 2014, 53, 856-860.
18. Y. Cao, X. Zhang, L. Tao, K. Li, Z. Xue, L. Feng and Y. Wei, *ACS Appl. Mater. Interfaces*, 2013, 5, 4438-4442.
19. M. Tao, L. Xue, F. Liu and L. Jiang, *Adv. Mater.*, 2014, 26, 2943-2948.
20. S. Zhang, F. Lu, L. Tao, N. Liu, C. Gao, L. Feng and Y. Wei, *ACS Appl. Mater. Interfaces*, 2013, 5, 11971-11976.
21. J. Zhang, S. Seeger, *Adv. Funct. Mater.*, 2011, 21, 4699-4704.
22. L. Wei, J. Zhang, B. Li and A. Wang, *J. Colloid Interf. Sci.*, 2014, 413, 112-117.
23. L. Zhang, Z. Zhang and P. Wang, *NPG Asia Mater.*, 2012, 4, e8.
24. N. A. Booker, D. Keir, A. J. Priestley, C. B. Ritchie, D. L. Sudarmana and M. A. Woods, *Water Sci. Technol.*, 1991, 23, 1703-1712.
25. J. D. Orbell, E. K. Tan, M. Coutts, S. W. Bigger and L. N. Ngeh, *Mar. Pollut. Bull.*, 1999, 38, 219-221.
26. Z. J. Wu, J. H. Wu, H. Xiang, M. S. Chun and K. Lee, *J. Colloid Surf. A*, 2006, 279, 167-174.
27. L. C. R. Machado, F. W. J. Lima, R. Paniago, J. D. Ardisson, K. Sapag and R. M. Lago, *Appl. Clay Sci.*, 2006, 31, 207-215.
28. Q. Zhu, F. Tao and Q. M. Pan, *ACS Appl. Mater. Interfaces*, 2010, 2, 3141-3146.
29. L. Wu, J. Zhang, B. Li and A. Wang, *Polym. Chem.*, 2014, 5, 2382-2390.
30. H. Lee, S. M. Dellatore, W. M. Miller and P. B. Messersmith, *Science*, 2007, 318, 426-430.
31. Y. Chen, H. Kim, *Appl. Surf. Sci.*, 2009, 255, 7073-7077.
32. S. H. Park, S. M. Lee, H. S. Lim, J. T. Han, D. R. Lee, H. S. Shin, Y. Jeong, J. Kim and J. H. Cho, *ACS Appl. Mater. Interfaces.*, 2010, 2, 658-662.
33. S. Wang, Y. Li, X. Fei, M. Sun, C. Zhang, Y. Li, Q. Yang and X. Hong, *J Colloid Interf. Sci.*, 2011, 359, 380-388.
34. Y. Liao, R. Wang and A. G. Fane, *J. Membr. Sci.*, 2013, 440, 77-87.
35. J. Hirschinger, D. Schaefer, H. W. Spiess and A. J. Lovinger, *Macromolecules*, 1991, 24, 2428-2433.
36. A. J. Lovinger, *Macromolecules*, 1982, 15, 40-44.
37. F. Liu, N. A. Hshim, Y. Liu, M. R. Moghareh Abed and K. Li, *J. Membr. Sci.*, 2011, 375, 1-27.
38. D. Wilson, M. A. Langell, *Appl. Surf. Sci.*, 2014, 303, 6-13.
39. A. Kihal, G. Fillion, B. Bouzabata and B. Barbara, *Phys. Status Solidi. B*, 2012, 249, 604-614.
40. J. H. Waite, M. L. Tanzer, *Science* 1981, 212, 1038-1040.
41. J. H. Waite, *Int. J. Adhes. Adhes.*, 1987, 7, 9-14.
42. J. H. Waite, X. X. Qin, *Biochemistry*, 2001, 40, 2887-2893.
43. J. Ryu, S. H. Ku, H. Lee, C. B. Park, *Adv. Funct. Mater.*, 2010, 20, 2132-2139.
44. B. Yu, D. A. Wang, Q. Ye, F. Zhou, W. M. Liu, *Chem. Commun.*, 2009, 6789-6791.
45. R. Liu, S. M. Mahurin, C. Li, R. R. Unocic, J. C. Idrobo, H. J. Gao, S. J. Pennycook, S. Dai, *Angew. Chem. Int. Ed.*, 2011, 50, 6799-6802.
46. T. Yamashita, P. Hayes, *Appl. Surf. Sci.*, 2008, 254, 2441-2449.
47. T. Fan, D. Pan and H. Zhang, *Ind. Eng. Chem. Res.*, 2011, 50, 9009-9018.
48. N. Eltouny, P. Ariya, *Ind. Eng. Chem. Res.*, 2012, 51, 12787-12795.
49. L. Zhang, J. Wu, Y. Wu, Y. Long, N. Zhao and J. Xu, *J. Am. Chem. Soc*, 2012, 134, 9879-9881.
50. J. Wu, N. Wang, Y. Zhao and L. Jiang, *ACS Appl. Mater. Interfaces*, 2012, 4, 3207-3212.
51. T. L. Sun, L. Feng, X. F. Gao and L. Jiang, *Acc. Chem. Res.*, 2005, 38, 644-652.
52. D. Quéré, *Annu. Rev. Mater. Res.*, 2008, 38, 71-99.
53. K. S. Liu, X. Yao and L. Jiang, *Chem. Soc. Rev.*, 2010, 39, 3240-3255.
54. R. N. Wenzel, *Ind. Eng. Chem.*, 1936, 28, 988-994.